Corrosion Science 53 (2011) 168–176

Contents lists available at ScienceDirect

Corrosion Science

journal homepage: www.elsevier.com/locate/corsci

A combined neural network and mechanistic approach for the prediction of corrosion rate and yield strength of magnesium-rare earth alloys

N. Birbilis [a,b,*,1], M.K. Cavanaugh [c,1], A.D. Sudholz [a,1], S.M. Zhu [b], M.A. Easton [b], M.A. Gibson [d]

[a] ARC Centre of Excellence for Design in Light Metals, Monash University, Australia
[b] CAST Co-operative Research Centre, Monash University, Australia
[c] Department of Materials Science and Engineering, The Ohio State University, USA
[d] CSIRO Division of Process Science and Engineering, Australia

ARTICLE INFO

Article history:
Received 13 July 2010
Accepted 3 September 2010
Available online 16 September 2010

Keywords:
A. Magnesium alloys
A. Rare earth
C. Corrosion
Yield strength
Neural network modelling

ABSTRACT

Additions of Ce, La and Nd to Mg were made in binary, ternary and quaternary combinations up to ~6 wt.%. This provided a dataset that was used in developing a neural network model for predicting corrosion rate and yield strength. Whilst yield strength increased with RE additions, corrosion rates also systematically increased, however, this depended on the type of RE element added and the combination of elements added (along with differences in intermetallic morphology). This work is permits an understanding of Mg–RE alloy performance, and can be exploited in Mg alloy design for predictable combinations of strength and corrosion resistance.

1. Introduction

The replacement of Fe-based alloys with Mg alloys can lead to substantial reductions in energy usage over the life cycle of automobiles [1]. The greatest benefits are achieved with the use of cast Mg alloys, particularly those produced by high-pressure die casting (HPDC) where the excellent castability of Mg can be exploited [2]. However, two of the key challenges for the uptake of Mg alloys are: (1) the inherent poor performance of the most common Mg–Al alloys at elevated temperatures typical of those required in applications such as automotive power-trains [3,4], and (2) the generally poor corrosion resistance of Mg alloys [5].

Mg alloys containing rare earths (RE) as the predominant alloying addition have been shown to possess superior creep resistance to other Mg alloys [6–10], particularly those based on the Mg–Al system; even when RE, Ca and/or Sr additions are made to Mg–Al alloys in an attempt to improve creep resistance [11]. Much of the work on creep-resistant Mg–RE alloys to date has revealed that REs behave differently, with Nd more effective than La and Ce in improving creep resistance. However, since Ce, La and Nd are the most common RE elements, typically found in misch-metal, the most cost effective alloys are to be derived from a combination of these elements, Therefore, it is necessary to have a detailed understanding of the combination of RE elements with respect to the key physical properties including corrosion rate and yield strength.

Initial studies have focused on the role of individual REs on the mechanical properties of binary Mg–RE alloys [12]. The REs investigated included Ce, La and Nd, which have different solubilities in Mg, viz. 0.23 wt.% for Ce, 0.74 wt.% for La and 3.6 wt.% for Nd. It was found that there is a strong relationship between the volume fraction of intermetallic compounds and the yield strength [13–14]. In fact, as a first approximation, the yield strength is a linear function of the amount of RE earth content in alloys. It is expected that a similar finding would occur for alloys containing multi-component RE alloys, since $Mg_{12}RE$ (where RE is Ce, La or Nd) is the stable phase in these alloys. The exception to this is that in cases where Nd is the sole or overwhelmingly dominate RE addition, Mg_3Nd may form instead of $Mg_{12}RE$ [13,14].

In addition, we have fundamentally characterised the corrosion and electrochemical properties of binary Mg–RE alloys [15]. It was shown that the electrochemistry of such alloys is rather complex, in that the relative increase in corrosion rate that occurs with increasing alloying addition was heavily influenced by the type of the intermetallic phase. It was determined from micro-capillary electrochemical studies that the corrosion rate (i_{corr}) was increased most remarkably with additions of Ce, followed by La and then Nd. This suggests that the corrosion of multi-component Mg–RE systems may be more complex, particularly if other impurity elements such as Fe, are also present. Fe is well known to have pro-

* Corresponding author at: ARC Centre of Excellence for Design in Light Metals, Monash University, Clayton, VIC 3800, Australia. Tel.: +61 3 9905 4919; fax: +61 3 9905 4940.
E-mail addresses: nick.birbilis@monash.edu, birbilis.1@osu.edu (N. Birbilis).
[1] These authors contributed equally.

0010-938X/$ - see front matter © 2010 Elsevier Ltd. All rights reserved.
doi:10.1016/j.corsci.2010.09.013

nounced effect on corrosion rate of alloys, and can be very difficult to control without the addition of Mn as used in Mg–Al alloys [16].

The interpretation of ternary and quaternary data is inherently challenging in an analytical sense, owing to the difficulty in accurately capturing the evolution of properties over a range of compositions (nominally 0–6 wt.%) for several different alloying elements. As a result, in order to manage the data in a holistic framework, we present the development of an artificial neural network (ANN) model for capturing the property evolution as a function of RE additions. One of the strengths of such a tool is that it can identify the key factors that affect a property and point researchers in the direction of the key mechanistic factors that affect that property, particularly for larger data sets.

In this paper, we extensively build on the fundamental knowledge gained from investigation of binary Mg–RE alloys to describe the evolution of corrosion rate and yield strength in ternary and quaternary Mg–RE alloys. These alloys represent a more realistic case for tangible automotive alloys, and such data has not been systematically presented before. It is posited that by understanding the interdependence between the evolution of strength and corrosion rate, more rational alloy development will occur, whilst also revealing fundamental aspects of Mg alloy corrosion.

2. Experimental methods

2.1. Alloy preparation

The Mg–RE alloys were produced from commercial purity Mg and RE metals, Ce, La and Nd. In addition to binary alloys, combinations of two and three of Ce, La and Nd, were added to Mg to make ternary and quaternary alloys. Whilst the binary alloys were made over a range of RE contents up to a nominal 6 wt.%, the ternary and quaternary alloys were made such that the nominal RE total was ~4 wt.%. The precise and relevant compositions of the alloys tested in this study are given in Appendix 1. In all cases, the composition was confirmed by using ICP-AES (Spectrometer Services, Coburg, Australia).

AM-cover® (0.2 wt.% tetrafluoroethane and 99.8 wt.% nitrogen gas) was used to protect the melt [17], which was held at a temperature of 740 °C within the crucible. Approximately 5 ppm Be from an Al–5Be master alloy was added to the alloys to assist with melt protection. The alloys were high-pressure die cast in a 250 tonne Toshiba cold chamber machine. The alloys were cast into a 3-cavity test bar die, consisting of two cylindrical 'dumbbell' and one flat test specimen. The round samples are 100 mm long and have a diameter in the gauge length of 6 mm. The flat specimen is 68 mm long and has dimensions of 6 × 3 mm within the gauge length. The ram velocity reached a maximum of 2.25 m/s, with a maximum pressure of almost 120 MPa and a biscuit size of 40 mm. Each shot took approximately 600 ms to fill the die cavity, and as a result of such rapid cooling rates, the microstructure of the castings was assumed to be more or less uniform.

2.2. Mechanical testing

Tensile tests of the round 'dumbbell' HPDC samples were conducted at room temperature using a screw driven Instron 4505 with a 100 kN load. A cross-head speed of 5 mm/min and an extensometer of gauge length 25 mm were used. Four repeats were performed per alloy composition.

2.3. Corrosion/electrochemical testing

Samples were cut from the HPDC specimens and ground to a 2400 grit finish. An electrochemical 'flat-cell' (PAR) was used with a working electrode area of 1 cm^2 exposed to a quiescent 0.1 M NaCl solution. The reference electrode used was a saturated calomel electrode (SCE). A VMP 3Z potentiostat. The open circuit potential was measured for 10 min prior to polarisation testing in order to establish an approximately stable potential. Potentiodynamic polarisation was performed using a sweep rate of 1 mV/s and tests were carried out in triplicate. The polarisation curves were used to i_{corr} (via a Tafel-type fit) using EC-Lab software. Such fitting is inherently difficult, however the ability of EC-lab to allow manual control is critical. As a general rule, fits were executed by selecting a portion of the curve that commenced >50 mV from E_{corr}, and i_{corr} was subsequently estimated from the value where the fit intercepted the potential value of the true E_{corr}. More generally, polarisation testing was also able to visually reveal comparative information related to the kinetics of anodic and cathodic reactions between alloys.

2.4. Microstructural analysis

SEM specimens were polished to a 1 μm diamond paste finish and imaged in backscattered electron mode using a JEOL JSM-7001F electron microscope, equipped with Bruker energy dispersive X-ray spectroscopy (EDX) analysis system.

2.5. ANN training

Artificial neural networks were trained for both yield strength and i_{corr} using JMP® 8 statistical software. Prior to training, four datasets were set aside for final independent testing of the resulting ANNs. Of the remaining datasets, 67% and 90% were used for training the ANNs for yield strength and i_{corr}, respectively, and the remainder was used for cross-validation.

3. Results and discussion

3.1. Typical microstructure of Mg–RE alloys

Increasing the total RE content generally increased the amount of intermetallic phase or eutectic observed within the alloys. Backscattered electron imaging was able to provide good contrast between the intermetallic phase, eutectic region, and the α-Mg grains. Typical microstructures observed in this work are seen in Fig. 1. These images are a selection from representative alloys that typify a binary, ternary and quaternary microstructure (with approximately ~3.5 wt.% total RE addition). Whilst it appears from low magnification SEM images that there is a continuous network of the intermetallic phase along the grain boundaries in the alloys, high magnification SEM reveals that this is generally not the case. What appear to be bulk intermetallic particles are, on a local scale, comprised of a eutectic mixture of the intermetallic phase and α-Mg (termed eutectic-α); as seen in Fig. 1 inserts.

As per binary Mg–RE alloys [13], the multi-RE alloys also have variations in the eutectic structure dependent upon the total alloy content and the proportion of the various RE elements that constitute that content. The binary Mg–La alloy has a lamellar eutectic. The addition of Ce leads to fibrous or rod-shaped α-Mg within the intermetallic, whilst alloys with increasing Nd content tend to present a 'divorced' eutectic. For the ternary and quaternary alloys, the intermetallic was confirmed to be $Mg_{12}RE$, with the REs being present interchangeably in this phase as shown by the EDX spectra, correspond to intermetallic and not the bulk alloy, in Fig. 1. Only in the binary Mg–Nd alloys was Mg_3Nd observed instead of $Mg_{12}RE$.

3.2. Strength of Mg–RE alloys

The yield strength as a function of the total wt.% RE from all the alloys tested in this study, including binary, ternary and quaternary combinations of Ce, La and Nd is shown in Fig. 2.

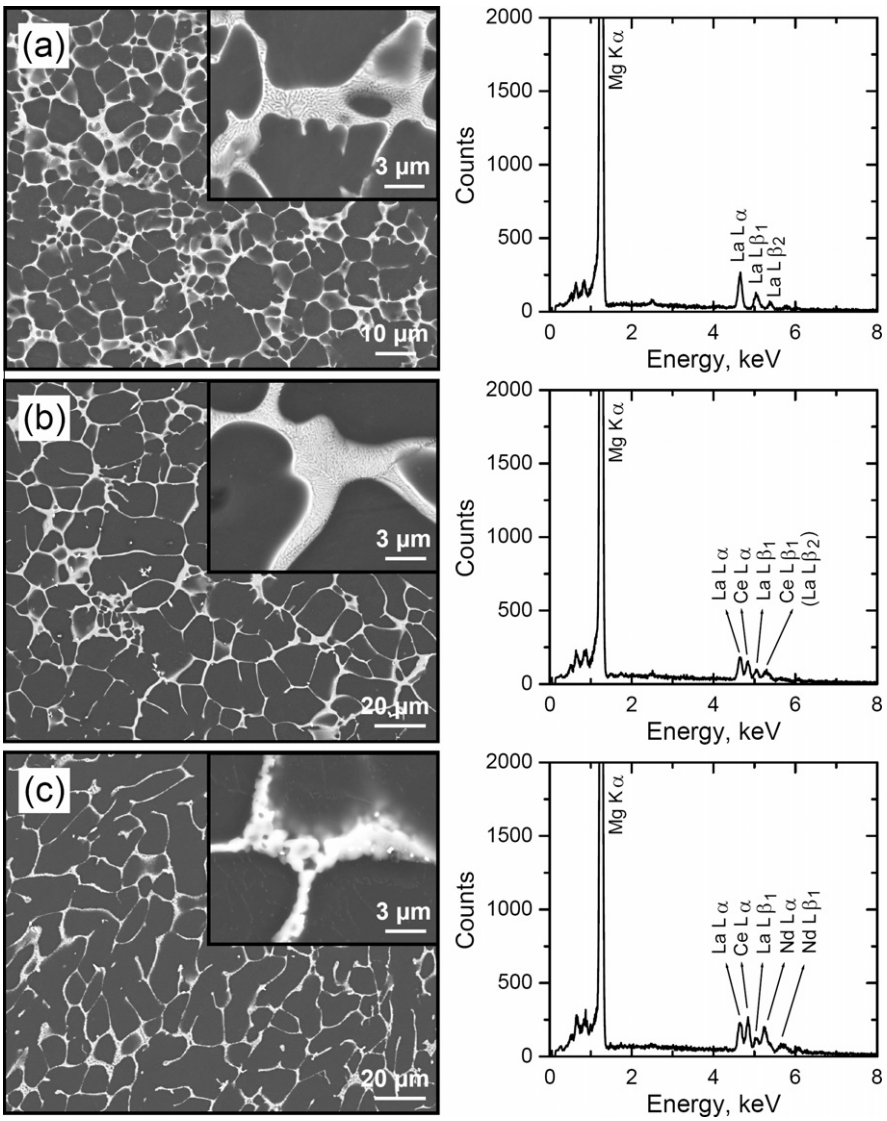

Fig. 1. A selection of backscattered SEM images of the general microstructure and EDX spectra from the associated intermetallic phase for die-cast (a) binary Mg-3.44La, (b) ternary Mg-1.89Ce-2.08La and (c) quaternary Mg-0.90Nd-1.78Ce-1.16La alloys (inserts are higher magnification micrographs showing the fine structure of the eutectic).

It can be seen that as the total wt.% RE alloying addition increases, the yield strength increases. The monotonic increase in yield strength relates very well with the wt.% RE additions, irrespective of the chemical type (i.e. Ce, La or Nd) of the alloying addition. The data contained in Fig. 2 will not be further analysed to isolate the effect of individual RE element additions as it represents a component of an ongoing investigation.

3.3. Corrosion of Mg–RE alloys

A summary of the corrosion rates observed for the Mg–RE alloys investigated (listed by alloy name) is shown in Fig. 3. There is a wide range of results contained in Fig. 3, with two key factors being apparent immediately: (1) All alloying additions increase i_{corr} beyond the value of pure Mg, and (2) A large spread in the i_{corr} values is seen, which is an indication of the ultra-sensitivity of Mg alloy corrosion rates to the type and amount of alloying additions present. Such a large spread of i_{corr} values is not nominally observed in other metal systems. The richness of the data contained in Fig. 3 is further rationalised by the discussion of the figures to follow. In addition, in order to reveal whether or not the spread of data seen

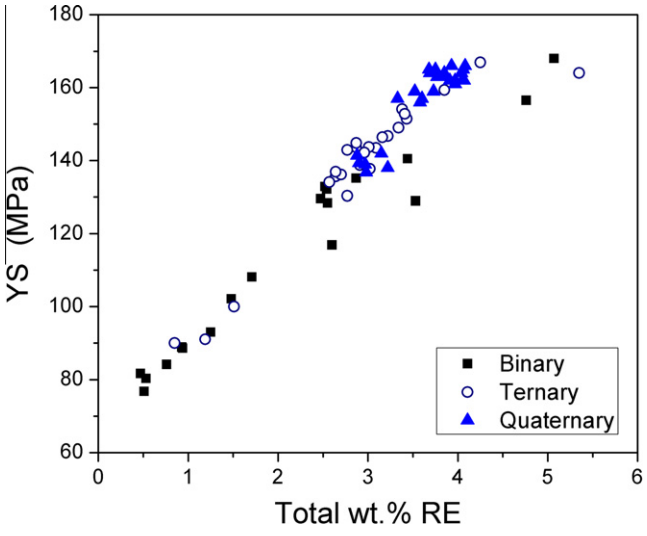

Fig. 2. Yield strength versus total alloy loading for Mg–RE alloys with various combinations of Ce, La and Nd.

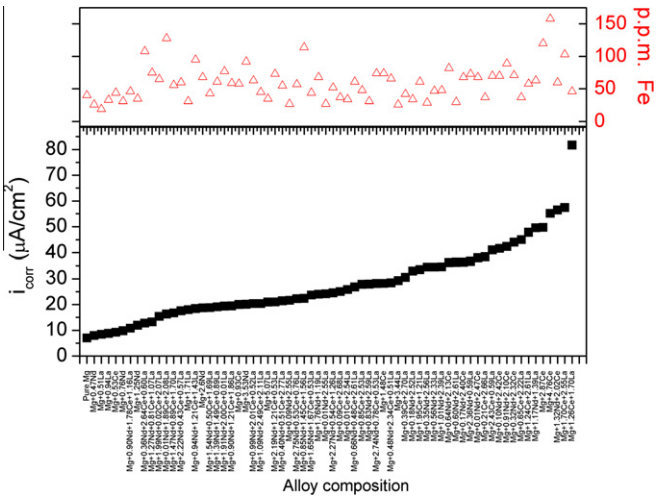

Fig. 3. Corrosion rate expressed as corrosion current density (i_{corr}) of a sorted list of the Mg–RE alloys tested herein. Data is presented with corresponding Fe impurity levels in parts per million.

in Fig. 3 is related to the Fe content and not the RE alloying addition, the corresponding impurity level of Fe is given. It is seen that no relationship exists with respect to Fe content. In this study, the Fe content is below what is a detrimental threshold and this is discussed further below.

Fig. 4 reveals the i_{corr} values as a function of the total wt.% RE alloying addition. This figure is analogous to that shown in Fig. 2, however, in this case, it is apparent that the observed behaviour is neither simple nor monotonic. It is observed is that for a given total wt.% RE (i.e. a given alloy loading) the resultant i_{corr} value can vary over a wide range. Further interpretation of Fig. 4 is facilitated by grouping the data according to the relative alloy complexity.

The results in Fig. 4 can be rationalised by consideration of the fact that different chemical types of RE have a marked difference on the electrochemical properties of the resulting alloy. Moreover, it is evident from a cursory visual inspection of Fig. 4 that quaternary alloys seem to allow for a greater total alloying additions to be made without a significant rise in i_{corr}. However, prior to discussing any mechanistic aspects, it is important to present the electrochemical data that will allow for a deeper discussion to ensue.

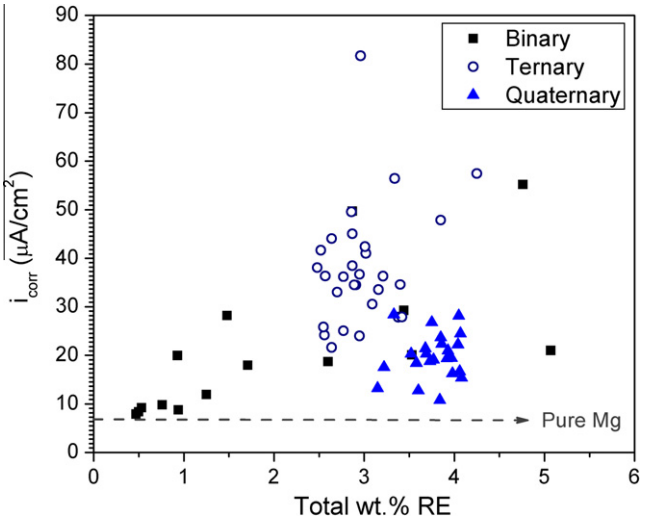

Fig. 4. Corrosion rate expressed as corrosion current density (i_{corr}) versus total alloy loading for Mg–RE alloys with various combinations of Ce, La and Nd.

3.4. Composition dependent properties

In order to help visualise the composition dependent spatial distribution of properties, modified ternary contour plots (generated using Origin 8®) are presented in Figs. 5 and 6 based on the empirical data.

To give a spread of data, the axis values have been modified and represent the data for a limited number of alloys that have a total RE composition of ~4 wt.% (+/− 0.3). As a result, the data depicted in the contour plots represents alloys with 96 wt.% Mg and a combination of REs adding to 4 wt.% (and hence the precise composition can be read from the plots).

What is observed from Figs. 5 and 6 is that as the contour becomes lighter, that the parameter of interest is increasing. For the development of strength, it appears from the contour plot that the optimum is realised when a combination of the RE elements are used, and that Nd has somewhat of a lower influence on development of strength than Ce and La. With respect to corrosion, we see that increasing Ce causes large increases in i_{corr}, as does La to a lesser extent. Increasing Nd on its own retains the (darker colored contour) relatively uniform i_{corr}, and again, some compromise is gained from a combination of the RE elements.

Whilst such observations can be made, they are somewhat qualitative in that one can already see that the attainment of quantitative information from ternary contour plots becomes difficult, and also, to fully quantify the data herein one would need a series of such plots at different iso-concentrations, or even quaternary plots, etc., making total data quantification unfeasible. This therefore points to the merits of ANN modelling for capturing large datasets and allow data analysis to occur by looking at the effect of the inputs over a range of compositions codependently.

3.5. Artificial neural network model development

Given the large amount of data collected herein, the information was packaged into a neural network model that could handle the multi-variables in composition (Mg, Ce, La, Nd and Fe) which dictate the outputs (yield strength, i_{corr}). In addition, such analysis will capture important aspects such as the specific role of the individual variables on properties, and, the precise composition that can deliver a specific set of properties.

The ANN structure for yield strength is shown in Fig. 7 and the equations for predicting the yield strength from wt.% RE can be found in Appendix B. For predicting strength, 3 nodes were required for ANN analysis, and hence 3 expressions (H1,...H3) contribute to the final formalism for YS. The ANN-predicted versus the observed yield strength is presented in Fig 8. The ANN was not only able to fit the training and validation data extremely well (R^2 = 0.98), but could also accurately predict for the test set (R^2 = 0.93).

To determine the effect each RE had on the yield strength, a fuzzy curve analysis was performed, shown in Fig. 9 (a detailed description of fuzzy curves and their construction can be found in [18]). Essentially, a fuzzy curve can reveal whether the membership of an element (input) is significant in the output [19] and was also demonstrated in [20]. If so, the fuzzy curve allows one to assess the relative significance an input (in this case RE content) has on the output (in this case, the yield strength). This relative significance is determined by the range the fuzzy curve spans on the C-axis, which is denoted in the legend of Fig. 9. Since it has been shown previously that any RE addition will improve the yield strength, an element with a greater influence (as deemed by the fuzzy curves) will be more efficient in increasing the yield strength. With La, having the largest fuzzy curve range, marginally has the most significant effect on the yield strength, and Nd (with the lowest fuzzy curve range) has the smallest effect on yield strength, but the three elements appear essentially comparable.

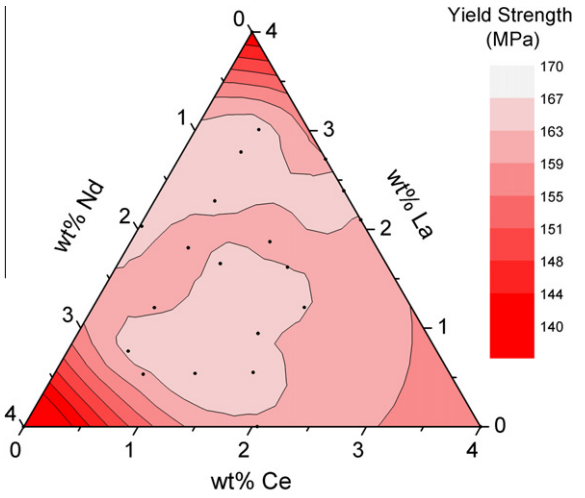

Figure 5.

Fig. 5. Contour plot of yield strength versus composition for Mg–Ce–La–Nd alloys with a total RE loading of ~4 wt.%.

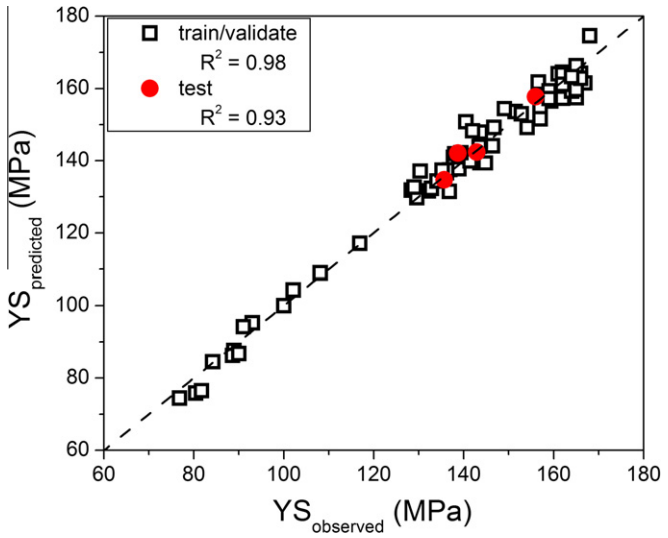

Fig. 8. ANN-predicted versus observed yield strength for both the training/validation and test sets.

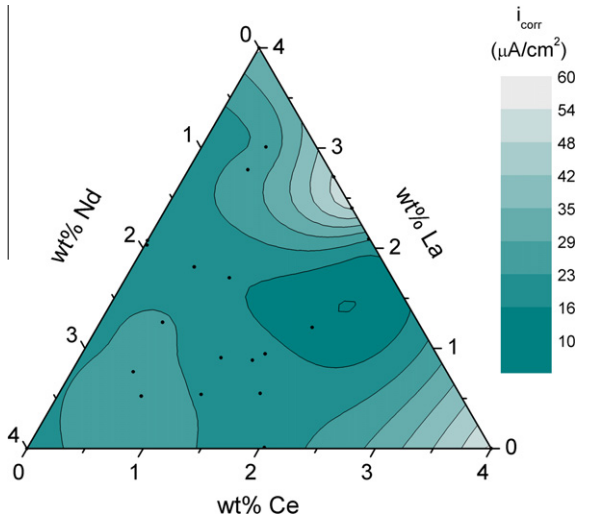

Fig. 6. Contour plot of corrosion rate (i_{corr}) versus composition for Mg–Ce–La–Nd alloys with a total RE loading of ~4 wt.%.

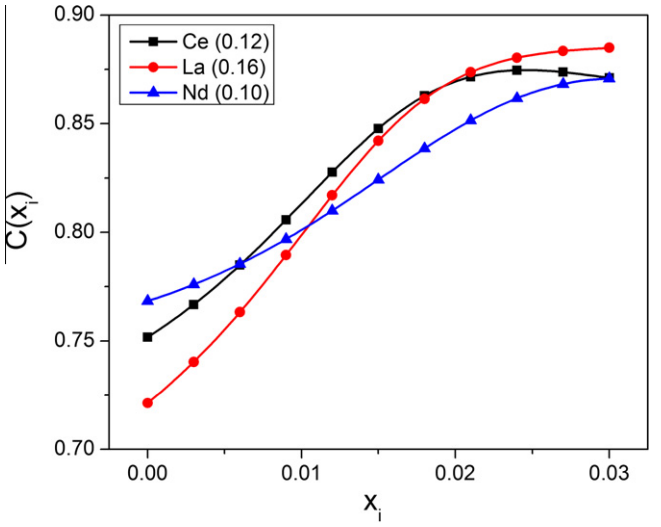

Fig. 9. Fuzzy curves for yield strength, where x_i is wt.% RE. The range of each fuzzy curve is indicated in the legend.

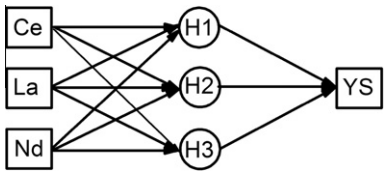

Fig. 7. ANN architecture used for modelling yield strength, which consisted of 3 inputs, a hidden layer with 3 nodes, and the output, yield strength, YS.

The i_{corr} ANN architecture used is shown in Fig. 10 and the equations for predicting i_{corr} are also included in Appendix B. The results of the trained ANN for i_{corr} are shown in Fig. 11. Although the R^2 values for the training/validation and test sets are noticeably lower for i_{corr} than those for yield strength, this correlation is quite good when considering the complexity of the electrochemistry that determines i_{corr} (will be discussed below, however the purpose of the ANN analysis here is to reveal that the ANN itself can point to mechanistic aspects independently). Again, fuzzy curve analysis was performed to establish the influence each RE has on i_{corr}. The fuzzy curves are presented in Fig. 12 and the range of each is indicated in the legend. Unlike the yield strength where a RE that has a strong effect is preferred, in the case of i_{corr}, the opposite is true. Since pure Mg was shown to have the lowest i_{corr}, any RE addition will increase i_{corr} and therefore, the RE element that has the smallest influence is most desirable. From the fuzzy curves, Nd not only has the least significance in determining i_{corr}, but the range is appreciably lower than either Ce or La (it is the range that is important herein and not the slope or direction). This suggests that additions of Nd can improve the yield strength (c/f. Fig. 9) without considerably increasing i_{corr}. Concomitantly we see that Ce is most effective at increasing i_{corr} from the ANN analysis. This analysis therefore adds huge value to the bulk data presented above (not to mention the expressions in Appendix B), where the large dataset alone (From Figs. 3–6) was unable to explicitly reveal such fine detail.

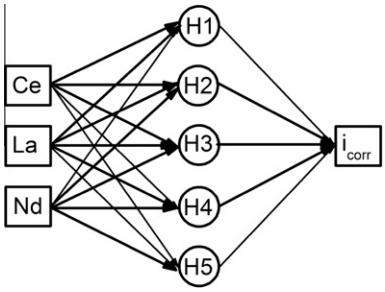

Fig. 10. ANN architecture used for modelling i_{corr}, which consisted of 3 inputs, a hidden layer with 5 nodes, and the output, i_{corr}.

In regards to corrosion, whilst Fig. 3 does not show any substantial relationship with Fe content, it was considered important to determine whether the neural network identifies any relationship with Fe. As confirmed by the fuzzy curves for i_{corr}, Fe has no measurable effect on the i_{corr} values determined herein for the range of Fe concentrations present in this study (up to 158 ppm).

4. Discussion

The data herein has shown that RE additions to Mg raise the yield strength; however simultaneously raise the corrosion rate. The individual RE elements were similar in the ability to increase strength, with La followed by Ce showing the greatest effect. The corrosion response was complex in that the respective REs had a different impact. We note from combining microstructural analysis and ANN modelling, that Ce is most detrimental for corrosion (increasing corrosion rate the fastest) and Nd is the least detrimental for corrosion (increasing corrosion rate the slowest). It was hence found that the optimum balance between the properties studied herein can come from the combination of the RE elements. The use of critical empirical data to develop such a predictive model shows that a powerful, multi-variable, model can be readily developed to aid in the role of optimised alloy development when complex parameter changes, such as those seen with i_{corr}, can occur. The expressions in Appendix B allow one to plot the variation in outputs for any input, essentially yielding a design tool. None the less, we can concede that we have not thus far defined the mechanistic aspects related to the response observed, and in order to justify the ANN model, we proceed to discuss mechanistic aspects below.

The basic influence of RE alloying additions on the corrosion of Mg can be understood by inspection of the raw polarisation curves, as shown in Figs. 13 and 14.

Inspection of the polarisation data presented in Fig. 13 explains the origin of the increase in i_{corr} as depicted in Fig. 4. Fig. 13 reveals that alloying significantly enhances the cathodic reaction kinetics which can be sustained by the alloy(s). The impact of increasing cathodic reaction (specifically hydrogen evolution) kinetics manifests as a movement of the cathodic branch to greater values (as denoted by the dashed line), which is consistent with ennoblement in the value of E_{corr}, but concomitant with a net increase in the i_{corr} value. It should be noted that RE additions do slow anodic reaction kinetics somewhat as also seen in Fig. 13, however, this is overwhelmed by the increase in cathodic reaction kinetics (meaning that the enhanced i_{corr} with RE additions appears to be dominated by the increase in cathodic reaction rates). As a result, this work reveals quite starkly that increasing RE additions enhances the cathodic reaction kinetics (via the introduction of Mg–RE intermetallic phases) and this in turn raises i_{corr}.

On the contrary, for quaternary alloying additions and few select other alloys which can be deduced from Fig. 3 (as Nd rich compositions), the increase in i_{corr} is subtle since there is a balance

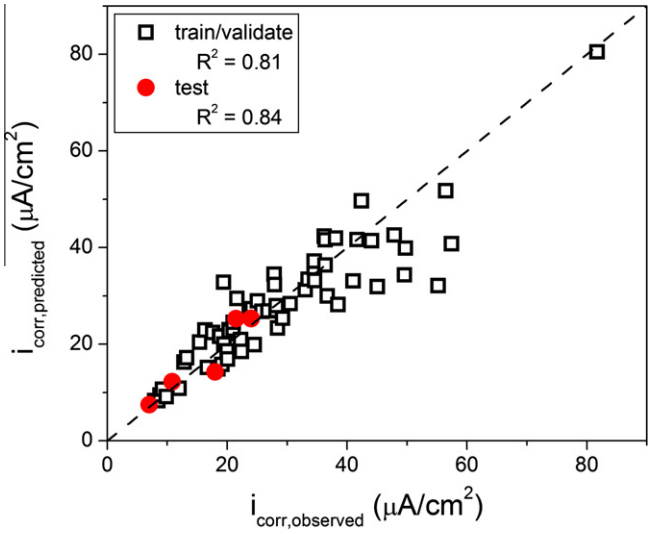

Fig. 11. ANN-predicted versus observed i_{corr} for both the training/validation and test sets.

between the net increase of cathodic reaction kinetics and decrease of anodic reaction rates. In our prior study that focused on binary Mg–RE alloys [14], we presented the polarisation curves of individual intermetallic compounds (IMs) which are not presented herein, but show that Mg_xRE_y IMs can sustain higher rates of cathodic reaction than Mg, are spontaneously passive, and also support low rates of anodic dissolution over the potential range characteristic of Mg–RE alloys. The ranking of such IMs in terms of their ability support cathodic reactions was Ce > La > Nd; whilst for anodic reactions it was seen that the lowest rates were Ce < La = Nd. This is in agreement with the observations in Fig. 14.

Whilst the individual electrochemistry of intermetallics is a useful aid, rationalising the mechanisms at play is also associated with the physical metallurgy of multi-element alloys, which can be complex. We recall that the intermetallic resides in a eutectic region that is in itself dual-phase (combining the IM and eutectic-α). Given however, the close relationship between RE elements in a physical metallurgy context, as seen in Fig. 1, RE elements form $Mg_{12}RE$ interchangeably, such that the IM actually contains any blend of REs (such that a better representation may actually be Mg_{12}(Ce,La,Nd)). Consequently intermetallic electrochemistry is complex. Another clue however, to the behaviour observed may reside in metallurgical calculations that dictate not only the volume percent $Mg_{12}RE$ itself being a function of the composition of the alloy, but the composition of the remnant α-Mg in the eutectic region of the alloy (the eutectic-α) [13]. Such information is seen in Fig. 15, and a trend, if not a relationship, is revealed – whereby the greater the percentage of RE in the eutectic-α the lower the i_{corr}. This would correspond to a situation whereby an RE loaded eutectic-α would support anodic dissolution reactions at lower rates than more pure Mg; hence counterbalancing the detrimental cathodic rate acceleration that occurs with the presence of $Mg_{12}RE$. Such a finding has not been previously reported, but can be quantified and rationalised from an electrochemical point of view (whereas from Fig. 2 it is clear that such chemistry specific intricacies are less important for development of yield strength). In fact, it is rather remarkable that such a small range of compositional change in the eutectic-α cause covers the large range of i_{corr} values observed. Such ultra-sensitivity to composition is however rationalised by inspection of the polarisation curves that show changes that impact anodic rate have a logarithmic relation and can hence cause disproportionately high reductions (but similarly enhancements) in rate. From inspection of the data and from a selection

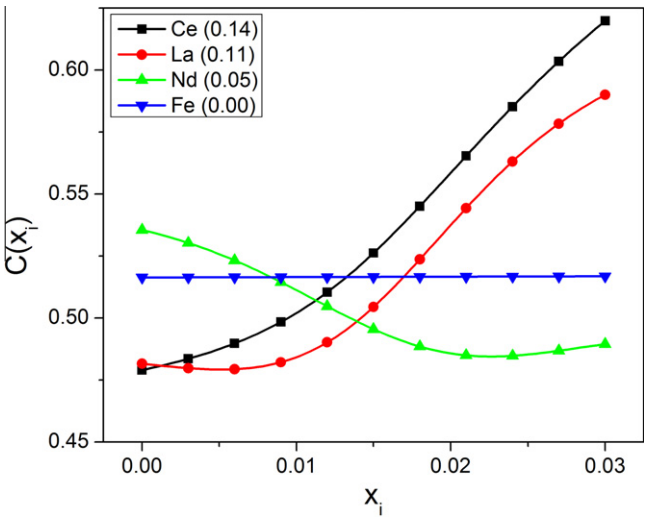

Fig. 12. Fuzzy curves for i_{corr}, where x_i is wt.%RE. The range of each fuzzy curve is indicated in the legend.

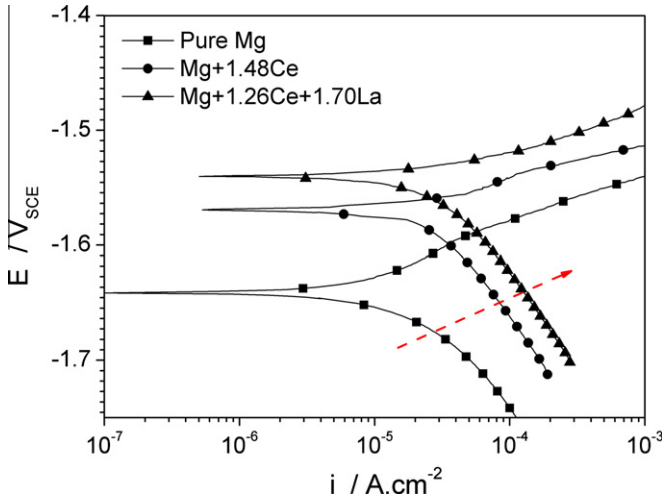

Fig. 13. Polarisation data for pure Mg and two Mg–RE alloys (in this case Mg-1.48Ce and Mg-1.26Ce-1.70La) in 0.1 M NaCl.

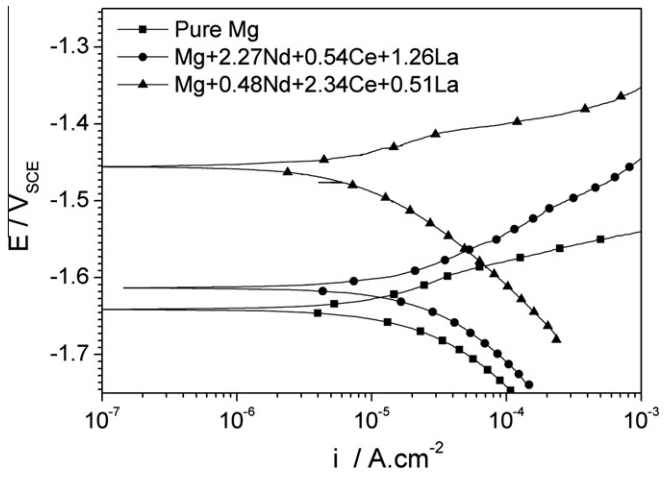

Fig. 14. Polarisation data for pure Mg and two Mg–RE quaternary alloys (in this case Mg-0.48Nd-1.78Ce-1.16La and Mg-2.27Nd-0.54Ce-1.26La) in 0.1 M NaCl.

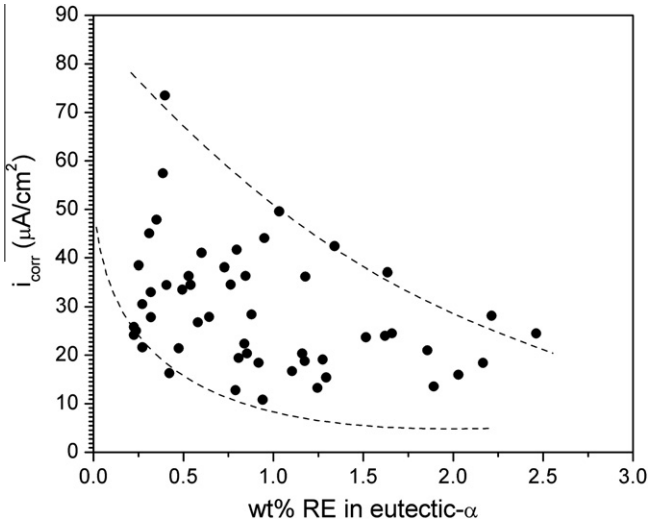

Fig. 15. Corrosion rate versus the "in solution" wt.% of RE in the eutectic α-Mg.

of micrographs, it becomes evident that when Nd is present, higher levels of RE in solute are possible, which is coupled with divorced eutectic morphology.

In addition there may be a minor effect – but likely important from a corrosion perspective – that a slightly higher amount of RE can remain in the bulk α-solid solution when Nd is present or in quaternary alloys (which must necessarily include Nd). In summary however the corrosion rate is ultimately a balance between the decreased anodic kinetics due to RE elements in solution in and the increase in cathodic kinetics from RE-containing intermetallic phases. The manipulation of this via the different eutectic morphologies and local composition (i.e. wt.% RE in euetctic-α) is responsible for the spread of data seen in i_{corr}. The ultimate value of i_{corr} and yield strength realised for any combination of RE additions can be readily predicted using ANN analysis – serving as an important alloy design tool.

5. Conclusion

The work presented herein has revealed a large body of previously unreported data pertaining to yield strength and i_{corr} of Mg–RE alloys. The breadth of data lends itself to integration into an ANN model framework that can harness the empirical data into a scientific tool. This allows for prediction and interpolation of both yield strength and i_{corr} values for alloys with any combination of Ce, La or Nd in a given composition window (up to 6 wt.% alloy loading by combination of the three RE elements).

The study shows that yield strength increases monotonically with increasing total RE content. Corrosion rates are, however, heavily dependent on both the type of RE element added and the amount of individual RE elements. We noted that RE additions tend to increase cathodic reaction kinetics owing to the development of a cathodic intermetallic second phase, and slightly decrease anodic reaction rates when present in solid solution. It was also shown that corrosion of Mg is ultra-sensitive to local composition, with a small variation in RE level in eutectic α covering the spectrum of corrosion rates observed.

ANNs for yield strength and i_{corr} determined that the three RE elements offered comparable improvements to the yield strength, but Nd additions did not adversely affect i_{corr}, to the extent that was observed for either La or Ce. Nd was able to favourably alter the eutectic morphology and the level of solute in the eutectic-α.

The highest alloy loading possible for improved strength, whilst retaining a minimal increase in i_{corr}, has been shown to be possible

through quaternary RE alloying additions. Nominally there is an inverse correlation between gaining favourable strength and favourable corrosion rates. The approach outlined herein shows how it may be possible to isolate regions of compositional space that make it possible to optimise (or at least 'trade off') both properties simultaneously.

This approach represents a useful design tool for Mg–RE alloys, whilst also demonstrating systematic alloy development strategy that can be applied generally in materials design with multi-property considerations.

Acknowledgements

The CAST Co-operative Research Centre was established under, and is funded in part by, the Australian Governments Co-operative Research Centres Scheme. The Australian Research Council (through the Centre of Excellence for Design in Light Metals) and the Victorian Government (through the Victorian Facility for Light Metals Surface Technology) are gratefully acknowledged. Maya Gershenzon and Andrew Yob are thanked for producing the samples. We thank the Monash Centre for Electron Microscopy for access to equipment.

Appendix A. Composition of alloys tested in this study

Alloy Composition in wt.% (Fe impurity level in parts per million)				
Ce	La	Nd	Mg	Fe (ppm)
0	0	0	100	40
0	0	0.47	99.53	26
0	0.51	0	99.49	19
0	0.94	0	99.06	33
0.53	0	0	99.47	44
0	0	0.76	99.24	31
1.78	1.16	0.9	96.16	46
0	0	1.25	98.75	35
2.64	0.6	0.36	96.4	108
0.81	1.07	1.27	96.85	75
0.02	2.07	1.99	95.92	65
1.89	2.08	0.01	96.02	128
0.89	1.7	1.47	95.94	56
0.43	0.57	2.22	96.78	60
0	1.71	0	98.29	31
1.21	1.43	0.94	96.42	95
0	0	2.6	97.4	68
0.5	1.69	1.54	96.27	43
1.49	0.89	1.39	96.23	61
2	0.01	1.91	96.08	77
1.21	0.9	1.86	96.03	59
0.93	0	0	99.07	58
0	0	3.53	96.47	92
2.01	0.52	0.99	96.48	63
2.49	2.11	1.09	94.31	45
0	5	0	95	35
1.21	0.53	2.19	96.07	73
0.51	2.77	0.4	96.32	55
0	2.55	0.09	97.36	27
0.53	0.76	2.75	95.96	57
1.45	0.85	1.56	96.14	114
1.67	0.53	1.65	96.15	44
0	1.9	1.76	96.34	68
0	2.55	0.01	97.44	27
0.54	1.26	2.27	95.93	52

Appendix A (*continued*)

Alloy Composition in wt.% (Fe impurity level in parts per million)				
Ce	La	Nd	Mg	Fe (ppm)
0.09	2.68	0	97.23	37
0.01	2.54	0	97.45	34
0.48	2.61	0.66	96.25	61
0.85	2.53	0	96.62	48
0.83	2.59	0	96.58	31
0.78	0.53	2.74	95.95	74
1.48	0	0	98.52	74
2.34	0.51	0.48	96.67	66
0	3.44	0	96.56	26
0.39	2.7	0	96.91	42
0	2.52	0.18	97.3	34
1.95	1.21	0	96.84	61
0	2.56	0.35	97.09	29
0	2.33	0.56	97.11	47
0	2.39	1.01	96.6	48
2.13	0	0.64	97.23	82
0	2.61	0.6	96.79	30
2.4	0	0.17	97.43	68
0	0.59	2.36	97.05	73
2.47	0	0.01	97.52	68
0.21	2.66	0	97.13	37
2.43	0.59	0	96.98	70
2.42	0	0.1	97.48	70
2.1	0	0.91	96.99	89
2.32	0	0.32	97.36	71
0.65	2.22	0	97.13	37
1.24	2.61	0	96.15	58
0	1.39	1.17	97.44	63
2.87	0	0	97.13	120
4.76	0	0	95.24	158
2.02	0	1.32	96.66	60
1.7	2.55	0	95.75	103
1.26	1.7	0	97.04	46

Appendix B. ANN-determined formulae for corrosion rate (i_{corr}) and yield strength (YS) as a function of composition in weight percent

$$i_{corr} = 10^{0.74-0.86H1 + 1.8H2-0.59H3 + 0.46H4 + 0.90H5}$$

$$H1 = \frac{1}{1+\exp(-3.3-2.5Ce+1.4La+1.8Nd)}$$

$$H2 = \frac{1}{1+\exp(-3.2-2.9Ce+0.35La+0.45Nd)}$$

$$H3 = \frac{1}{1+\exp(-17-5.5Ce+4.8La+4.8Nd)}$$

$$H4 = \frac{1}{1+\exp(-12-3.2Ce+0.63La+5.4Nd)}$$

$$H5 = \frac{1}{1+\exp(-5.8-4.6Ce+1.1La+2.9Nd)}$$

$$YS = 10^{1.78-0.32H1+0.39H2+0.20H3}$$

$$H1 = \frac{1}{1+\exp(-0.16-0.62Ce+0.75La+2.3Nd)}$$

$$H2 = \frac{1}{1+\exp(-0.52-1.2Ce+0.92La+0.25Nd)}$$

$$H3 = \frac{1}{1+\exp(-2.2-0.33Ce+0.41La+0.77Nd)}$$

References

[1] M. Hakamada, T. Furuta, Y. Chino, Y. Chen, H. Kusuda, M. Mabuchi, Energy 32 (2007) 1352–1360.
[2] J.F. King, Mater. Sci. Technol. 23 (2007) 1–14.
[3] P. Humble, Mater. Forum 21 (1997) 45–56.
[4] A. Luo, Int. Mater. Rev. 49 (2004) 13–30.
[5] K.U. Kainer (Ed.), Magnesium–Alloys and Technology, Wiley-VCH, Germany, 2003.
[6] B.R. Powell, V. Rezhets, M.P. Balogh, R.A. Waldo, JOM 54 (8) (2002) 34–38.
[7] S.M. Zhu, M.A. Gibson, J.F. Nie, M.A. Easton, P. Bakke, in: M.O. Pekguleryuz, N.R. Neelameggham, R. Beals, E.A. Nyberg (Eds.), Magnesium Technology 2008, The Metals Minerals and Materials Society, Warrendale, PA, 2008, pp. 437–440.
[8] C.J. Bettles, C.T. Forwood, D.H. StJohn, M.T. Frost, D.S. Jones, M. Qian, G.L. Song, J.R. Griffiths, J.F. Nie, in: H.I. Kaplan (Ed.), Magnesium Technology 2003, The Metals, Minerals and Materials Society, Warrendale, PA, 2003, pp. 223–226.
[9] P. Lyon, J.F. King, K. Nuttall, in: G.W. Lorimer (Ed.), Proceedings of the Third International Magnesium Conference, Institute of Materials, UK, 1996, pp. 99–108.
[10] I.P. Moreno, T.K. Nandy, J.W. Jones, J.E. Allison, T.M. Pollock, Scripta Mater. 45 (2001) 1423–1429.
[11] B.R. Powell, V. Rezhets, M.P. Balogh, R.A. Waldo, in: J. Hryn (Ed.), Magnesium Technology 2001, The Minerals, Metals and Materials Society, Warrendale, PA, 2001, pp. 175–182.
[12] S.M. Zhu, M.A. Gibson, J.F. Nie, M.A. Easton, T. Abbott, Scripta Mater. 58 (2008) 477–480.
[13] T.L. Chia, M.A. Easton, S.M. Zhu, M.A. Gibson, N. Birbilis, J.F. Nie, Intermetallics 17 (2009) 481–490.
[14] L.L. Rokhlin, Magnesium alloys containing rare earth metals, Taylor & Francis, New York, USA, 2003.
[15] N. Birbilis, M.A. Easton, A.D. Sudhloz, S.M. Zhu, M.A. Gibson, Corros. Sci. 51 (2009) 683–689.
[16] J.D. Hanawalt, C.E. Nelson, J.A. Peloubet, Trans. AIME 147 (1942) 273.
[17] S.P. Cashion, N.J. Ricketts, The Conference of Metallurgists, The Metallurgical Society of CIM, Toronto, Canada, 2001.
[18] Y. Lin, G.A. Cunningham, IEEE Trans. Fuzzy Syst. 3 (1995) 190.
[19] V. Novak, A. Perfilieva, J. Mockor, Mathematical principles of fuzzy logic, Kluwer, Dordrecht, Netherlands, 1999.
[20] M.K. Cavanaugh, R.G. Buchheit, N. Birbilis, Corros. Sci. 52 (2010) 3070–3077.